(Preprint) AAS 12-164

DESIGN OF OPTIMAL TRANSFERS BETWEEN NORTH AND SOUTH POLE-SITTER ORBITS

Jeannette Heiligers,[*] Matteo Ceriotti,[†] Colin R. McInnes,[‡] and James D. Biggs[§]

Recent studies have shown the feasibility of an Earth pole-sitter mission, where a spacecraft follows the Earth's polar axis to have a continuous, hemispherical view of one of the Earth's Poles. However, due to the tilt of the polar axis, the North and South Poles are alternately situated in darkness for long periods during the year. This significantly constrains observations and decreases mission scientific return. This paper therefore investigates transfers between north and south pole-sitter orbits before the start of the Arctic and Antarctic winters to maximize scientific return by observing the polar regions only when lit. Clearly, such a transfer can also be employed for the sole purpose of visiting both the North and South Poles with one single spacecraft during one single mission. To enable such a novel transfer, two types of propulsion are proposed, including solar electric propulsion (SEP) and a hybridization of SEP with solar sailing. A direct optimization method based on pseudospectral transcription is used to find both transfers that minimize the SEP propellant consumption and transfers that trade-off SEP propellant consumption and observation time of the Poles. Also, a feedback control is developed to account for non-ideal properties of the solar sail. It is shown that, for all cases considered, hybrid low-thrust propulsion outperforms the pure SEP case, while enabling a transfer that would not be feasible with current solar sail technology.

INTRODUCTION

Previous and current missions aiming at observing the polar regions include NASA's ICESat-1 mission (2003 – 2010)[1] and ESA's Cryosat-2 mission (2010 – ongoing)[2]. Both missions aim (or aimed) at measuring the changes and trends in the ice fields in order to determine the environmental, economical and political consequences on a global scale. However, both satellites orbit(ed) the Earth in a low Earth orbit (LEO) with repeat ground tracks of 91 and 369 days, respectively, with sub-cycles of 30 and 33 days that provide uniform coverage of the polar regions. Still, in order to obtain a full, hemispherical view of the polar re-

[*] Ph.D. Candidate, Advanced Space Concepts Laboratory, Department of Mechanical and Aerospace Engineering, University of Strathclyde, 75 Montrose Street, Glasgow G1 1XJ, Scotland, United Kingdom.
[†] Research Fellow, Advanced Space Concepts Laboratory, Department of Mechanical and Aerospace Engineering, University of Strathclyde, 75 Montrose Street, Glasgow G1 1XJ, Scotland, United Kingdom.
[‡] Director, Advanced Space Concepts Laboratory, Department of Mechanical and Aerospace Engineering, University of Strathclyde, 75 Montrose Street, Glasgow G1 1XJ, Scotland, United Kingdom.
[§§] Associate Director, Advanced Space Concepts Laboratory, Department of Mechanical and Aerospace Engineering, University of Strathclyde, 75 Montrose Street, Glasgow G1 1XJ, Scotland, United Kingdom.

gions, data obtained during different passages (and therefore at different times) need to be combined. This results in a very poor temporal resolution that is not sufficient for particular applications of polar observation such as meteorological forecasting and space weather monitoring, both of which require continuous monitoring of the polar regions. Additionally, with recent changes to the polar ice packs, new shipping routes open up that require continuous high-latitude communication links. Note that these communication links cannot be provided by spacecraft in geostationary orbit (GEO) as these high latitudes are out of sight for GEO spacecraft.[3]

In response to the need for continuous, hemispherical coverage of the polar regions, alternative concepts can be found in literature such as extended Molniya orbits[4], where the critical inclination of the classical Molniya orbit is increased to 90° using low-thrust propulsion, and pole-sitter platforms[5-7]. The latter involve a spacecraft that maintains a fixed location over one of the Earth's Poles. It can therefore be seen as an analogue to the geostationary orbit for polar observation. According to Lazzara[8] such a vantage point would allow the identification and tracking of storm systems, to generate atmospheric motion vectors, to contribute to space weather monitoring and to provide the critical high-latitude communication links mentioned before.

Being on a non-Keplerian orbit, a pole-sitter spacecraft requires a continuous, thrust-induced acceleration in order to counterbalance the gravitational attraction of the Earth and Sun while following the Earth's polar axis during the year. To this aim, previous research by Ceriotti and McInnes[6] considered two different propulsion strategies, including the use of solar electric propulsion (SEP) and a hybridization of SEP with a solar sail. In case of the latter, the idea is that, by combining these two particular types of propulsion system the disadvantages of the separate propulsion systems cancel out.[9] This novel concept has already shown highly promising results for a range of applications such as interplanetary transfers[10], periodic orbits in the vicinity of the Lagrange points of the Earth-Moon system[11], displaced geostationary orbits[12] and artificial equilibria in the Earth-Sun three body-problem[13, 14].

For both types of propulsion strategies, Ceriotti and McInnes[6] have demonstrated the existence of minimum SEP propellant pole-sitter orbits by varying the Earth-spacecraft distance during the year, while constraining the spacecraft to follow the Earth's polar axis. Comparing the results in terms of initial mass required to carry a fixed payload mass showed that the hybridized case allows for propellant savings over the pure SEP case, thereby enabling longer missions. Subsequent work by Ceriotti and McInnes[7] included an investigation of the control of the pole-sitter orbit under unexpected conditions such as injection errors and temporary SEP thruster failure and resulted in the design of an effective feedback control system.

The work in this paper elaborates on the research performed so far for the pole-sitter concept and attempts to provide a solution for potential restrictions in the observations that can be performed from a pole-sitter position. The issue is that, in order to limit the acceleration required to maintain the pole-sitter position, the minimum Earth-spacecraft distance is 1.5 million km. At such a large distance, the available resolution is limited. Still, in the visible range of the spectrum, a resolution of a few kilometres should be possible and would among others allow for the observation of dynamic phenomena and large-scale polar weather systems.[15] However, due to the tilt of the polar axis, the polar regions are alternately situated in darkness for long periods during the year. Clearly, for observations in the visible spectrum, this significantly constrains observation and limits the scientific return of the mission. To overcome this problem, this paper investigates transfers between pole-sitter orbits above the North and South Poles before the start of their respective winters such that unfavourable conditions above one of the Poles are exchanged for favourable conditions above the opposite Pole.

In addition to the increased scientific return that these transfers can establish they can clearly serve an additional purpose. While polar observations from LEO cannot provide the continuous coverage required for a range of applications, they do have the advantage of visiting both the North and South Poles with one single spacecraft. A similar mission objective can be achieved for the pole-sitter spacecraft by dividing the mission into segments where each segment is devoted to the observation of one of the Earth's Poles and the mission segments are linked through the north to south pole-sitter transfers designed in this paper.

Corresponding to previous work on pole-sitter orbits, the transfers will be investigated for the use of both pure SEP and hybridized SEP and solar sailing. In both cases the SEP propellant consumption will be

minimized. For both propulsion strategies the optimal control problem is defined and solved using a direct optimization method based on pseudospectral transcription. Initial guesses are generated using an inverse method by first assuming a particular shape for the trajectory that satisfies the boundary constraints and subsequently solving for the thrust profile required to follow that trajectory. Results are obtained for both short and long duration transfers where the first visits each of the Poles within one year, while the latter visits both Poles within 3 years. Initial results will show that an opportunity exists to not only minimize the SEP propellant consumption, but also the useful observation time per Pole. Through a weighted-sum approach of the separate objectives in the objective function a trade-off between propellant consumption and time spent in each of the pole-sitter orbits can then be established. Finally, a feedback control system is designed to show the feasibility of the transfers even when a non-ideal solar sail is considered.

The structure of the paper is as follows. First, a detailed definition of the pole-sitter orbit and the reference frame in which it is defined will be provided. Subsequently, the need for the transfer between north and south pole-sitter orbits will be underlined. In the subsequent section, the optimal control problem will be defined and the direct method used to solve it is described. Also the inverse method applied to generate appropriate initial guesses is provided. Then, the results for the pure SEP case will be presented, followed by the results for the hybrid low-thrust case, including a detailed comparison between the performance of the two different propulsion strategies. Finally, a section will be devoted to the feedback control required to enable the transfer in case of non-ideal sail properties and at the end of the paper the conclusions will be drawn.

POLE-SITTER ORBIT

The pole-sitter orbit is defined in the Earth-Sun circular restricted three body problem (CR3BP). The CR3BP describes the motion of a negligibly small mass, m (spacecraft), in the gravitational field of two massive masses, m_1 and m_2 (i.e. Sun and Earth), that are assumed to move in circular orbits about their common center of mass. The barycentric rotating reference frame commonly employed is shown in Figure 1 and shows its rotation about the z axis, $\boldsymbol{\omega}$, that is equal to the angular rate of the Earth's motion around the Sun. Furthermore, the (x, y) plane is parallel to the ecliptic, the x axis points in the direction of the Earth and the y axis completes the Cartesian right handed system. New units are introduced as follows: the sum of the masses of the two massive bodies is taken as the unit of mass and the distance between them as the unit of length. Then, with the mass ratio $\mu = m_2/(m_1 + m_2)$ the positions of m_1 and m_2 along the x axis become $-\mu$ and $1-\mu$, respectively. Finally, $1/\omega$ is chosen as unit of time, causing $\omega = 1$.

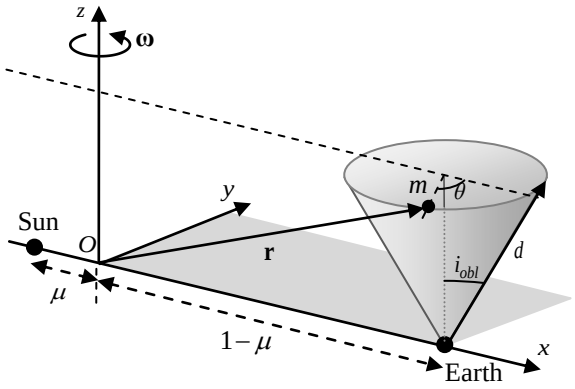

Figure 1 Schematic of (north) pole-sitter orbit and reference frame.

The dynamics of a spacecraft in this reference frame are described by the following set of differential equations:

$$\ddot{\mathbf{r}} + 2\boldsymbol{\omega} \times \dot{\mathbf{r}} = -\nabla U + \mathbf{a} \tag{1}$$

with U a potential combining the gravitational potential and a potential that represents the centripetal acceleration:

$$U = -(1-\mu)/r_1 - \mu/r_2 - \left(x^2 + y^2\right)/2 \tag{2}$$

where $\mathbf{r}_1 = \mathbf{r} + \begin{bmatrix} \mu & 0 & 0 \end{bmatrix}^T$ and $\mathbf{r}_2 = \mathbf{r} - \begin{bmatrix} (1-\mu) & 0 & 0 \end{bmatrix}^T$ are the Sun-spacecraft and Earth-spacecraft position vectors, respectively.

Depending on the type of propulsion employed the thrust-induced acceleration, $\mathbf{a}$, is given by:

$$\mathbf{a} = \begin{cases} \dfrac{\mathbf{T}}{m} & \text{SEP} \\ \dfrac{\mathbf{T}}{m} + \beta_0 \dfrac{m_0}{m} \dfrac{\mu_S}{r_1^2} \left(\hat{\mathbf{n}} \cdot \hat{\mathbf{r}}_1\right)^2 \hat{\mathbf{n}} & \text{Hybrid propulsion} \end{cases} \tag{3}$$

with $\mathbf{T}$ the SEP thrust vector, m the instantaneous mass of the spacecraft, the subscript '0' indicating the start of the mission, μ_S the gravitational parameter of the Sun and $\hat{\mathbf{n}}$ the unit vector in the direction of the solar radiation pressure acceleration generated by the solar sail. Note that this paper initially assumes a perfectly reflecting (i.e. an ideal) solar sail, causing $\hat{\mathbf{n}}$ to be directed normal to the sail's surface. Later on in the paper, the influence of non-ideal properties of the solar sail will be investigated. Finally, β is the sail lightness number, which is a characteristic of the solar sail and can be defined as the ratio of the solar radiation pressure acceleration and the solar gravitational acceleration, or equivalently as a function of the sail area to spacecraft mass ratio.[16]

Due to the consumption of propellant by the SEP system, the dynamics in Eq. (1) need to be augmented with the following differential equation for the spacecraft mass:

$$\dot{m} = -\frac{T}{I_{sp} g_0} \tag{4}$$

with I_{sp} the specific impulse of the SEP thruster and g_0 the Earth standard gravitational acceleration.

Using the SEP thruster or the hybrid propulsion system, the motion of the spacecraft in the CR3BP can be enforced to follow the polar axis. Figure 1 shows that, due to the obliquity of the ecliptic, i_{obl}, and the rotation of the reference frame, the Earth's polar axis describes a cone during the year and the spacecraft needs to track this apparent (clockwise) motion of the polar axis. Therefore, for a *constant* Earth-spacecraft distance, d, the state vector of the spacecraft, $\mathbf{x} = \begin{bmatrix} x & y & z & \dot{x} & \dot{y} & \dot{z} \end{bmatrix}^T$, is prescribed by:

$$\mathbf{x}_{North} = \begin{bmatrix} d \sin i_{obl} \cos\theta + (1-\mu) \\ -d \sin i_{obl} \sin\theta \\ d \cos i_{obl} \\ -d \sin i_{obl} \sin\theta \\ -d \sin i_{obl} \cos\theta \\ 0 \end{bmatrix}, \qquad \mathbf{x}_{South} = \begin{bmatrix} d \sin i_{obl} \cos(\theta+\pi) + (1-\mu) \\ -d \sin i_{obl} \sin(\theta+\pi) \\ -d \cos i_{obl} \\ -d \sin i_{obl} \sin(\theta+\pi) \\ -d \sin i_{obl} \cos(\theta+\pi) \\ 0 \end{bmatrix} \tag{5}$$

where the subscripts 'north' and 'south' indicate a pole-sitter above the North and South Poles, respectively, and θ is the instantaneous angular position of the spacecraft along the north pole-sitter orbit measured

from winter solstice, as shown in Figure 1. However, previous work by Ceriotti and McInnes[6] also considered *variable* altitude pole-sitter orbits that are more fuel optimal. These allow the Earth-spacecraft distance to vary during the year according to the following sinusoidal law:

$$d(\theta) = d_0 + (d_1 - d_0)\frac{1-\cos\theta}{2} \tag{6}$$

with d_0 and d_1 the distances from the Earth at winter and summer solstices, respectively, see Figure 2.

Note that, in the rest of the paper we conventionally refer to the four seasons in the northern hemisphere, so winter is the period from the 21st December to 21st March, and so on.

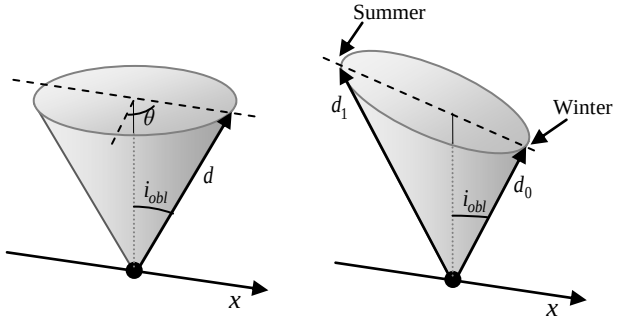

Figure 2 Schematic of constant and variable altitude pole-sitter orbits.

TRANSFER BETWEEN POLE-SITTERS

In order to underline the need for a transfer between north and south pole-sitter orbits, Figure 3a shows the elevation, ε, of the Sun at the North Pole and the Arctic circle (i.e. at a latitude of $\lambda = 66.5°$). The top plot clearly shows that, for the North Pole, the Sun does not rise above the horizon from autumn equinox (September) to spring solstice (March) and during that time the North Pole is permanently dark. Clearly, a similar plot but mirrored in the x-axis can be generated for the South Pole. Furthermore, the bottom plot illustrates the commonly known fact that the Arctic circle marks the edge of the region where the Sun does not rise above the horizon for a full day at least once per year. The light and dark conditions of the North and South Poles can also be illustrated in the CR3BP, see Figure 3b, which shows that light conditions occur when the polar axis is tilted towards the Sun, while darkness dominates when the polar axis is tilted away from the Sun.

In the introduction of the paper it was already stated that sufficient resolution from the pole-sitter orbits can only be obtained in the visible range of the electromagnetic spectrum, see Reference 15 for a detailed discussion. The dark conditions on the North and South Poles therefore severely restrict these observations, leading to a loss in the mission scientific return. A solution to this issue would be if the spacecraft follows the north pole-sitter orbit from March to September and then transfers to the south pole-sitter orbit to observe the South Pole from September to March.

Depending on the time allowed to perform this transfer, two types of transfers can be defined: a short duration transfer and a long duration transfer. The short duration transfer considers flight times of less than half a year and leaves the north pole-sitter orbit between summer solstice ($t = \pi$) and autumn equinox ($t = \frac{3}{2}\pi$) and enters the south pole-sitter between autumn equinox ($t = \frac{3}{2}\pi$) and winter solstice ($t = 2\pi$), see Figure 4. Since the transfer cannot be performed instantly, the observation time per Pole will always be less than half a year, resulting in the fact that the Poles cannot be viewed throughout the period when lighting conditions occur. For this to be possible, the long-duration transfer is defined. Then, the spacecraft leaves the north pole-sitter between autumn and winter and with a transfer time of half to one year the spacecraft enters the south pole-sitter between summer and autumn. Then, the observation time per Pole is

also half a year to one year, where a one year observation time automatically implies that part of the observations are performed when the polar regions are in darkness.

Note that due to the symmetry of the problem, the transfers designed to transfer from a north pole-sitter to a south pole-sitter can also be employed to transfer from south to north. This paper therefore only provides the results for the north to south pole-sitter transfer.

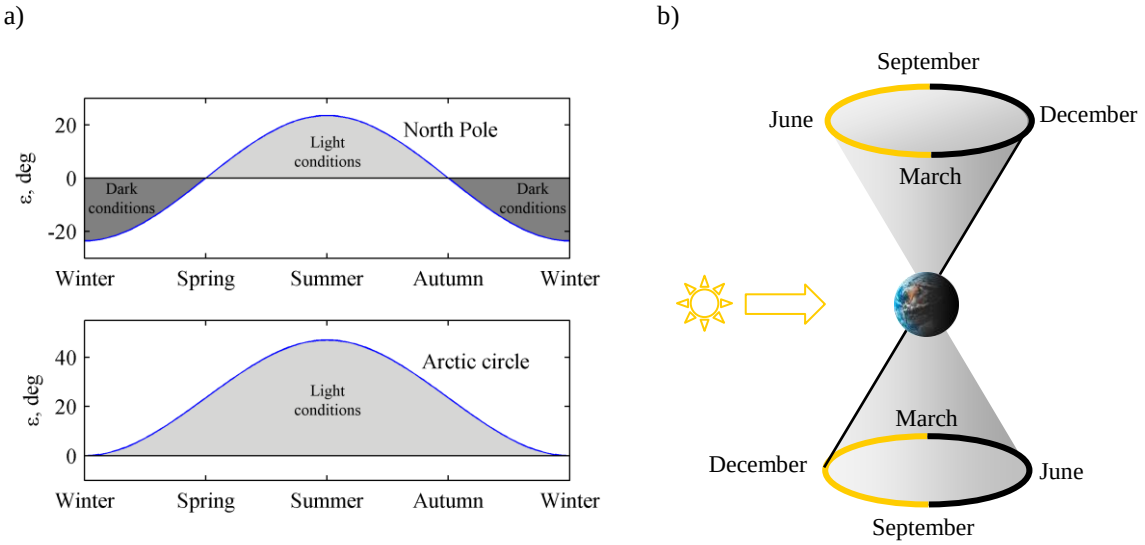

Figure 3 Solar elevation angle at the North Pole and Arctic circle (a) and schematic of dark (black line) and light (yellow line) conditions on the North and South Poles during the year (b).

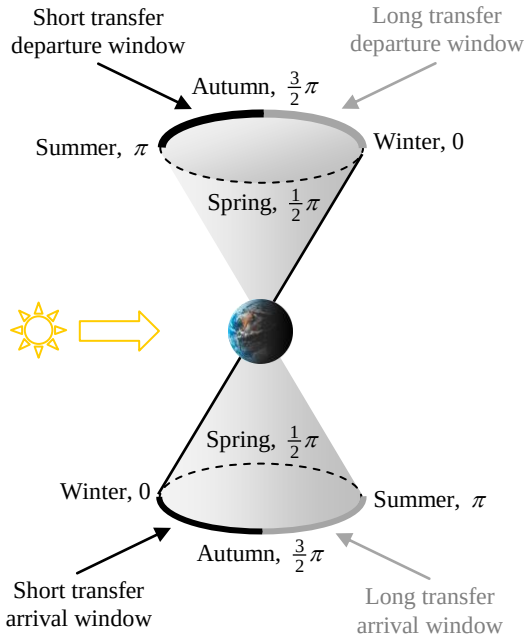

Figure 4 Illustration of the departure and arrival conditions in the north and south pole-sitter orbits for the short and long duration transfers.

OPTIMAL CONTROL PROBLEM

In order to design and optimize the short and long duration transfers defined in the previous section, the optimal control problem in the respective transfer needs to be solved. In general, an optimal control problem is to find a state history $\mathbf{x}(t) \in \mathbb{R}^{n_x}$ and a control history $\mathbf{u}(t) \in \mathbb{R}^{n_u}$, $t \in \left[t_0, t_f\right]$ that minimizes the cost function:

$$J = \phi\left(\mathbf{x}_0, \mathbf{x}_f, t_0, t_f\right) + \int_{t_0}^{t_f} L\left(\mathbf{x}(t), \mathbf{u}(t), t\right) dt \tag{7}$$

while satisfying the dynamics

$$\dot{\mathbf{x}}(t) = \mathbf{f}\left(\mathbf{x}(t), \mathbf{u}(t), t\right) \tag{8}$$

and the constraints

$$\mathbf{c}(\mathbf{x}, \mathbf{u}, t) \leq 0 \tag{9}$$

These constraints can include event constraints on the initial and final states and time, bounds on the state and control variables and time and path constraints. The first term on the right hand side of Eq. (7) is the endpoint (Mayer type) cost function, which is only a function of the initial and final states and time, while the second term is the Lagrange cost function and is a function of time.

Initially, the objective for the transfer between the pole-sitters is to minimize the propellant consumption. The cost function therefore equals:

$$J = -m_f \tag{10}$$

Note that, later on in the paper this cost function will be expanded to allow for a more detailed analysis. The state vector was already previously defined when introducing Eq. (5), but is expanded here to include the mass of the spacecraft: $\mathbf{x} = \begin{bmatrix} x & y & z & \dot{x} & \dot{y} & \dot{z} & m \end{bmatrix}^T$. Clearly, the initial and final state vectors should coincide with the conditions in the north and south pole-sitter orbits at the initial and final times of the transfer. For the constraint on the initial mass of the spacecraft it is assumed that the spacecraft is injected into the pole-sitter orbit at winter solstice with a mass of 1000 kg (see Reference 6). From this, the mass at the start of the transfer can be computed by assuming that the transfer is initialized in the first year after pole-sitter orbit insertion.

The control vector can take two different forms, depending on the type of propulsion system employed. For the pure SEP case, the control vector contains the Cartesian thrust components of the SEP thruster in the CR3BP reference frame, $\mathbf{u} = \begin{bmatrix} T_x & T_y & T_z \end{bmatrix}^T$. This control vector is expanded to also include the Cartesian components of the sail normal vector in case hybrid propulsion is employed: $\mathbf{u} = \begin{bmatrix} T_x & T_y & T_z & n_x & n_y & n_z \end{bmatrix}^T$. Note that for both control vectors the Cartesian components rather than two thrust angles and the thrust magnitude are used to prevent ambiguities.[17] This, however, requires the following path constraints to ensure that the combined SEP thrust vector does not exceed the maximum thrust magnitude and to ensure that the norm of the sail normal vector equals unity:

$$\sqrt{T_x^2 + T_y^2 + T_z^2} \leq T_{\max}, \quad \sqrt{n_x^2 + n_y^2 + n_z^2} = 1 \tag{11}$$

Clearly, the second path constraint only holds for a hybrid propulsion transfer, in which case an additional path constraint needs to be enforced, as the solar sail can only produce an acceleration pointing away from the Sun. The corresponding path constraint is:

$$\left(\hat{\mathbf{n}} \cdot \hat{\mathbf{r}}_1\right) \geq 0 \tag{12}$$

Finally, to constrain the optimal solution to either the short or long duration transfer illustrated in Figure 4, the following bounds are defined for the initial time, t_0, and final time, t_f:

$$\left.\begin{aligned} \pi \le t_0 &\le \tfrac{3}{2}\pi \\ \tfrac{3}{2}\pi \le t_f &\le 2\pi \end{aligned}\right\} \text{ Short transfer} \qquad \left.\begin{aligned} \tfrac{3}{2}\pi \le t_0 &\le 2\pi \\ 3\pi \le t_f &\le \tfrac{7}{2}\pi \end{aligned}\right\} \text{ Long transfer} \tag{13}$$

Optimal control solver

To solve the optimal control problem defined above, a direct method is employed that is based on pseudospectral transcription and is implemented in the open source software tool PSOPT.[18] PSOPT discretizes the time interval into a finite number of collocation points and Legendre or Chebyshev polynomials are used to approximate the time dependent variables at the collocation points. This way, the infinite dimensional optimal control problem is transformed into a finite dimension non-linear programming (NLP) problem, which is solved using the software package IPOPT (Interior Point OPTimizer).[19] The advantage of using pseudospectral methods is that the derivatives of the state functions at the nodes are computed by matrix multiplication only and any integral associated with the problem is approximated using well known Gauss quadrature rules.

Initial guess

In order to initialize the optimization, PSOPT requires a first guess. For this, an inverse method is adopted by first assuming a particular shape for the trajectory (that satisfies the boundary constraints), and subsequently analytically computing the SEP thrust vector components required to follow that shape from the equations of motion. Note that the initial guess assumes the use of only the SEP thruster.

The boundary conditions are the starting point for the shape proposed here. The initial and final state vectors are assumed to be fixed and coincide with the north and south pole-sitter orbits in the following way: $x_0 = x_f$, $y_0 = -y_f$ and $z_0 = -z_f$ and therefore $\dot{x}_0 = -\dot{x}_f$, $\dot{y}_0 = \dot{y}_f$ and $\dot{z}_0 = -\dot{z}_f$, see Figure 5. Subsequently, a parabolic velocity profile is assumed in between the initial and final state vectors:

$$\dot{\mathbf{r}}(t) = \mathbf{a}t^2 + \mathbf{b}t + \mathbf{c} \tag{14}$$

with $\mathbf{r} = \begin{bmatrix} x & y & z \end{bmatrix}^T$ the position vector, the overhead dot indicating the derivative with respect to time and $\mathbf{a}$, $\mathbf{b}$ and $\mathbf{c}$ vectors of constants. From the initial and final velocity conditions it can be shown that $\mathbf{c} = \dot{\mathbf{r}}_0$ and $\mathbf{b} = \frac{1}{t_f}\left(\dot{\mathbf{r}}_f - \dot{\mathbf{r}}_0\right) - \mathbf{a}t_f$ with the subscripts ‘ 0 ’ and ‘ f ’ indicating the conditions at the initial and final times. By integrating Eq. (14) the following shape for the position vector can be found:

$$\mathbf{r}(t) = \mathbf{a}\left(\frac{1}{3}t^3 - \frac{1}{2}t_f t^2\right) + \frac{1}{2t_f}\left(\dot{\mathbf{r}}_f - \dot{\mathbf{r}}_0\right)t^2 + \dot{\mathbf{r}}_0 t + \mathbf{d} \tag{15}$$

Again, from the initial and final position conditions it can be shown that $\mathbf{d} = \mathbf{r}_0$ and $\mathbf{a} = -\frac{6}{t_f^3}\left(\mathbf{r}_f - \mathbf{r}_0 - \frac{1}{2}\left(\dot{\mathbf{r}}_0 + \dot{\mathbf{r}}_f\right)t_f\right)$. Finally, differentiating Eq. (14) gives the profile of the acceleration vector, resulting in the following final position, velocity and acceleration profiles:

$$\mathbf{r}(t) = -6\frac{\mathbf{r}_f - \mathbf{r}_0 - \frac{1}{2}(\dot{\mathbf{r}}_0 + \dot{\mathbf{r}}_f)t_f}{t_f^3}\left(\tfrac{1}{3}t^3 - \tfrac{1}{2}t_f t^2\right) + \frac{1}{2t_f}(\dot{\mathbf{r}}_f - \dot{\mathbf{r}}_0)t^2 + \dot{\mathbf{r}}_0 t + \mathbf{r}_0$$

$$\dot{\mathbf{r}}(t) = -6\frac{\mathbf{r}_f - \mathbf{r}_0 - \frac{1}{2}(\dot{\mathbf{r}}_0 + \dot{\mathbf{r}}_f)t_f}{t_f^3}\left(t^2 - t_f t\right) + \frac{1}{t_f}(\dot{\mathbf{r}}_f - \dot{\mathbf{r}}_0)t + \dot{\mathbf{r}}_0 \qquad (16)$$

$$\ddot{\mathbf{r}}(t) = -6\frac{\mathbf{r}_f - \mathbf{r}_0 - \frac{1}{2}(\dot{\mathbf{r}}_0 + \dot{\mathbf{r}}_f)t_f}{t_f^3}\left(2t - t_f\right) + \frac{1}{t_f}(\dot{\mathbf{r}}_f - \dot{\mathbf{r}}_0)$$

The required thrust profile to execute this shape-based transfer can now easily be extracted from the equations of motion by substituting Eqs. (16) and (3) into Eq. (1) and rewriting for the thrust vector, $\mathbf{T}$.

In order to obtain an approximation for the mass profile during the transfer, the initial guess defined in Eq. (16) is discretized into a set of nodes that are equally distributed along the transfer. The mass profile at the i_{th} node is then approximated through the following recurrence relation that assumes a constant thrust magnitude during the time in between two consecutive nodes, Δt:

$$m_{i+1} = m_i - \frac{T_i}{I_{sp} g_0}\Delta t \qquad (17)$$

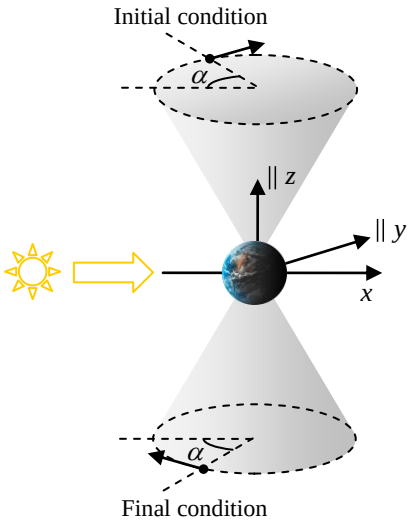

Figure 5 Definition of initial and boundary conditions for the initial guess

SOLAR ELECTRIC PROPULSION TRANSFERS

Using the initial guess defined in the previous section, this section starts with generating propellant optimum transfers between north and south pole-sitter orbits using only the SEP thruster. Corresponding to the work in Reference 6, two test cases are considered: transfers between constant altitude pole-sitter orbits with an Earth-spacecraft distance of 0.01 AU and transfers between variable altitude pole-sitter orbits with $d_0 = 0.01$ AU and $d_1 = 0.018$ AU. Furthermore, the specific impulse of the SEP thruster is assumed to be 3200 s and a maximum SEP thrust magnitude of $T_{\max} = 0.25$ N is adopted.

Minimum propellant transfers

Figure 6 provides the results for the constant altitude pole-sitter orbit. Both the results for the short and long transfers are provided, which require a propellant consumption of 21.3 and 22.8 kg, respectively. The declination plots in Figure 6c and Figure 6d show that the pole-sitter spacecraft correctly follows the declination of the Sun and also clearly show the difference between the short and long duration transfers: while the short duration transfer observes both the North and South Poles for a short period every year (95 days per Pole, see the arrows on the time axis), the long-duration transfer allows to observe both Poles every three years but for a much longer duration (244 days per Pole). However, as was already previously stated, part of these observations are taken during a negative solar declination, i.e. when the Poles are in darkness.

For the variable altitude pole-sitter, similar results can be obtained, see Figure 7. Comparing the results with the constant altitude pole-sitter orbit shows that the transfer for the variable altitude pole-sitter orbit requires less propellant: 12.4 and 19.7 kg for the short and long transfers, respectively. However, this gain in propellant mass comes at the cost of a decrease in the observation time per Pole: 63 and 214 days.

In both cases (i.e. the constant and variable altitude pole-sitters), the short duration transfer slightly outperforms the long transfer in terms of propellant consumption, despite the higher initial mass at the start of the transfer as the short transfer is initiated before the long duration transfers, see Figure 4. This is convenient, because it means that the short transfer is very suitable for the previously defined additional mission objective of observing both the North and South Poles with one single spacecraft.

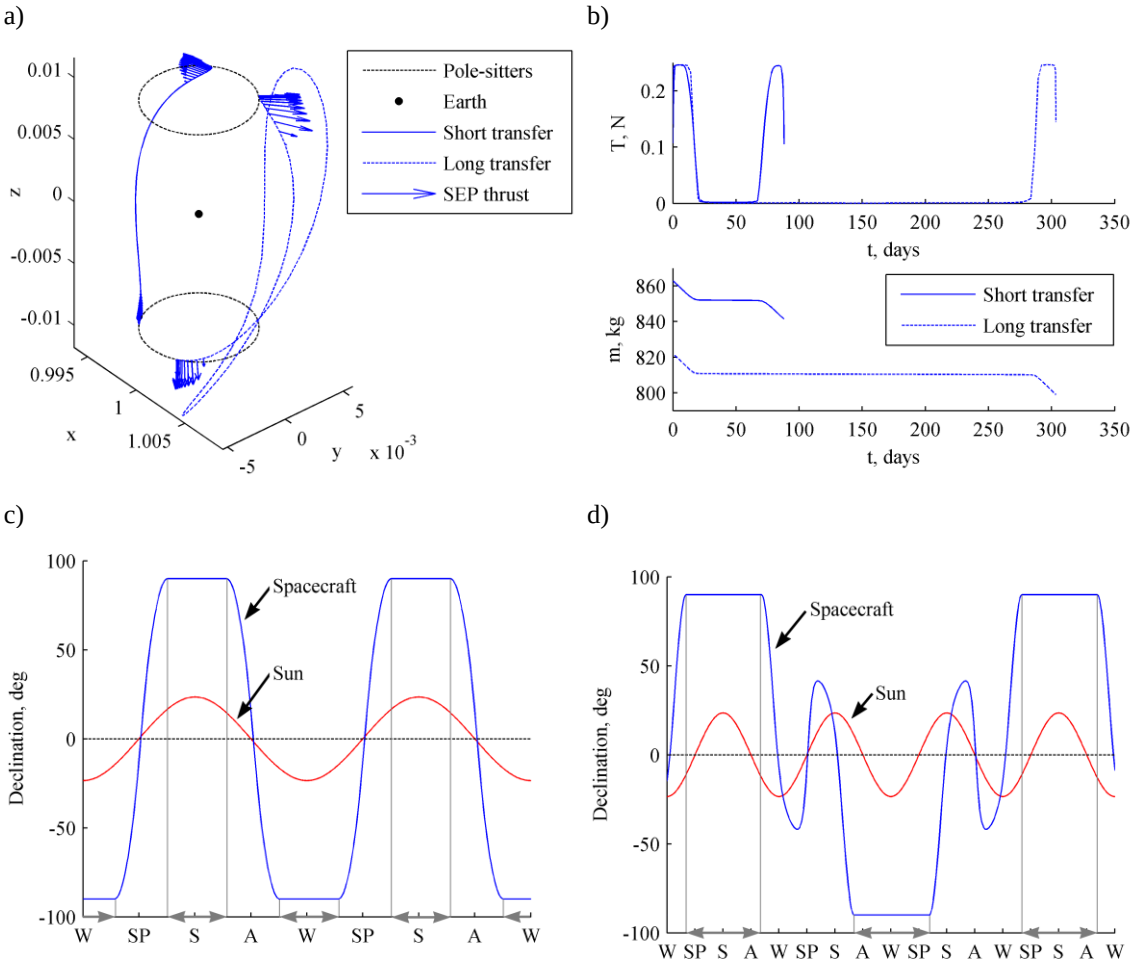

Figure 6 Minimum propellant transfers between constant altitude pole-sitters. Transfers in CR3BP reference frame (a). SEP thrust profiles (b). Declination plots for short (c) and long (d) transfers.

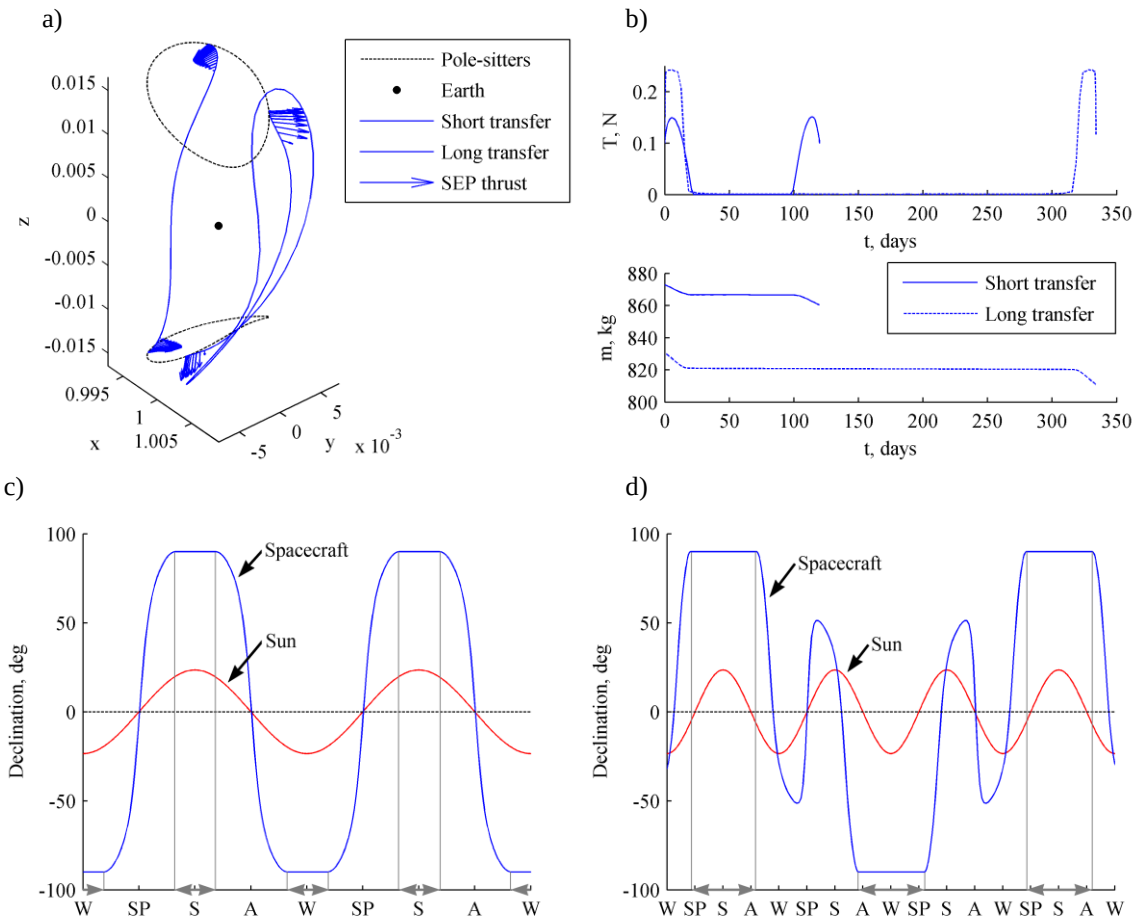

Figure 7 Minimum propellant transfers between variable altitude pole-sitters. Transfers in CR3BP reference frame (a). SEP thrust profiles (b). Declination plots for short (c) and long (d) transfers.

Minimum propellant, maximum observation time transfers

In the design of the minimum-propellant transfers presented in the previous subsection, the observation time of the polar regions is not taken into account. However, if the purpose of the transfer is to enable observations of the Poles in light conditions only, it can be concluded that the observation time for the short transfer is very limited, see Figure 6c and Figure 7c. Therefore, in order to increase the time spent above each of the Poles, additional optimizations have been carried out that involve the two conflicting objectives of minimum SEP propellant consumption and maximum observation time per Pole (or equivalently minimum transfer time). In order to consider both objectives a weighted sum approach is used in the definition of the objective function:

$$J = \frac{m_f - m_0}{m_0} + w\frac{t_f - t_0}{2\pi} \tag{18}$$

The results for the short transfer are provided in Figure 8 for both the constant and variable altitude pole-sitter orbits. The plots show that, as expected, increasing the weight factor, w, increases the observation time per Pole but at the cost of additional propellant. For a propellant mass increase of 16.9 and 29.5 kg the observation time is increased with 32 and 49 days for the constant and variable altitude pole-sitter orbits, respectively. The figure furthermore shows that an upper bound exists for the propellant mass and observation time. This bound is reached when the spacecraft thrusts continuously at maximum thrust mag-

nitude along the transfer. In that case, the time of flight cannot be reduced any further despite increasing the weight factor in the objective function.

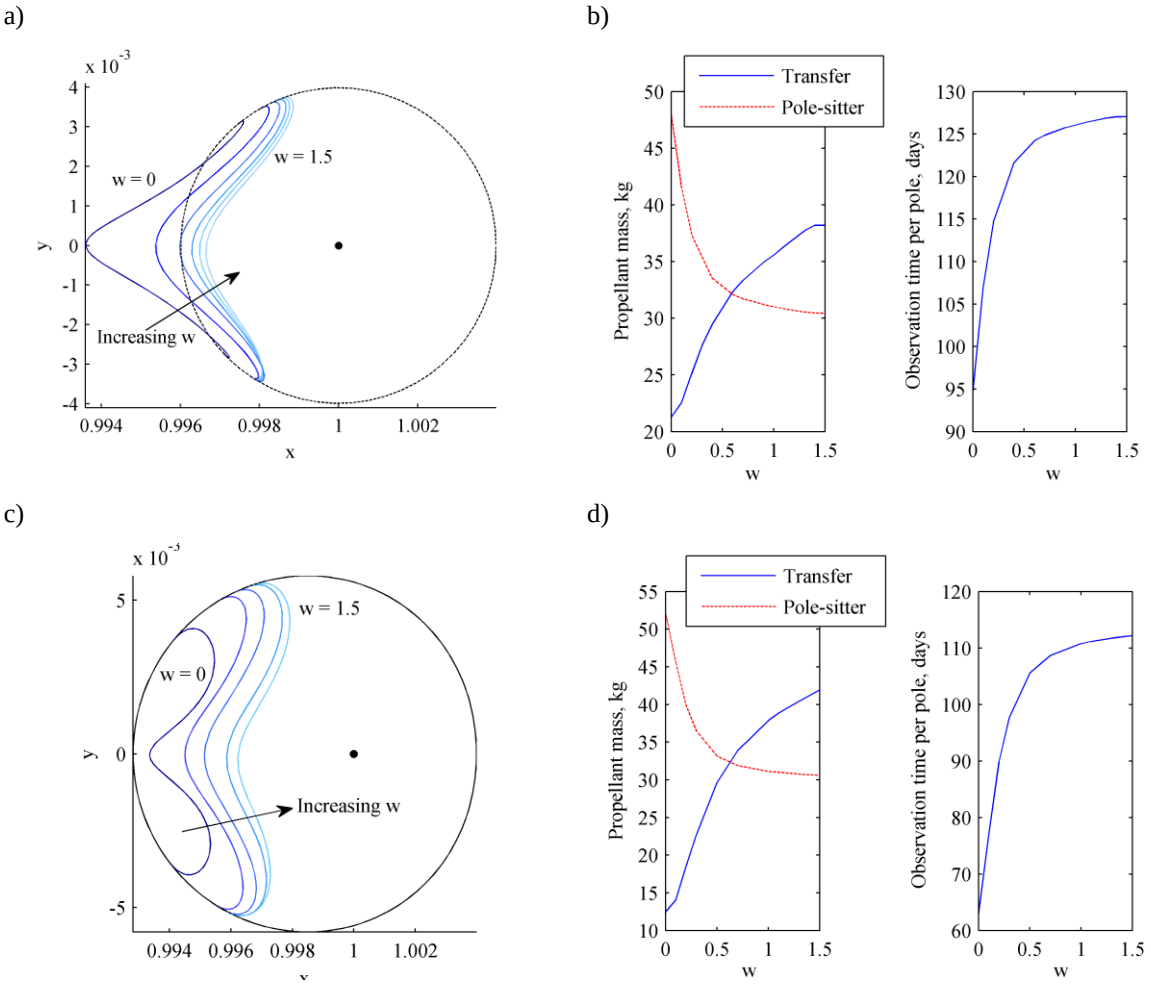

Figure 8 Short transfers between constant (a,b) and variable (c,d) altitude pole-sitters optimized for a weighted sum of the SEP propellant consumption and the observation time per Pole. Transfers in CR3BP reference frame (a,c) and propellant consumption and observation time as function of the objective function weight (b,d).

In order to put the demand on the SEP thruster for performing these transfers in perspective, Figure 8b and Figure 8d also provide the amount of propellant that would be required if the spacecraft stayed in the pole-sitter orbit, rather than transferring to the pole-sitter on the other side of the ecliptic. Note that, corresponding to the assumption for the transfer, this propellant mass is computed during the first year of the pole-sitter mission. For both the constant and variable altitude pole-sitter orbits it becomes clear that, for small values of the weight factor, it is more expensive to stay in the pole-sitter than to perform the transfer, i.e. for $w \leq 0.59$ and $w \leq 0.63$, respectively. This implies that the transfer could enable a possible extension of the pole-sitter mission lifetime. Only for large values of the weight factor, the propellant consumption in the transfer exceeds that of the pole-sitter orbit itself.

Similar results as in Figure 8 are obtained for the long duration transfer in Figure 9. Note that different values for the weight factor are employed, because the transfer times increase with respect to the short transfer while the propellant consumption is of the same order of magnitude. Again, at the cost of an increase in the propellant consumption of 13.9 and 17.1 kg the observation time can be increased by 121 and

151 days for the constant and variable altitude pole-sitter orbits, respectively. And again, an upper bound exists for the propellant mass and observation time. In this case, this upper bound is imposed by the minimum transfer time of half a year. The figure finally shows that for all weight factor values it is more convenient to perform the transfer than to stay in the pole-sitter orbit during the time of the transfer.

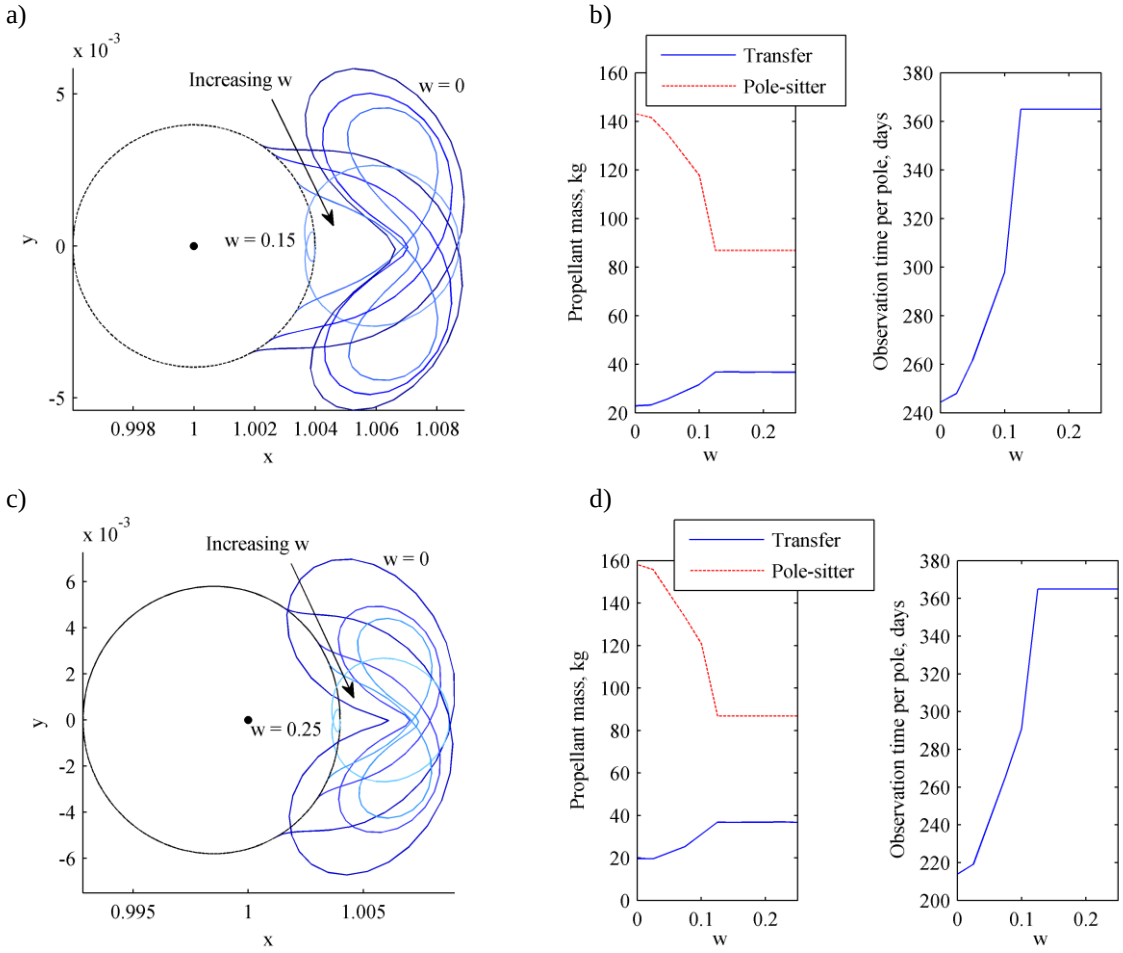

Figure 9 Long transfers between constant (a,b) and variable (c,d) altitude pole-sitters optimized for a weighted sum of the SEP propellant consumption and the observation time per Pole. Transfers in CR3BP reference frame (a,c) and propellant consumption and observation time as function of the objective function weight (b,d).

HYBRID PROPULSION TRANSFERS

In order to improve the performance of the transfers presented in the previous section, this section provides the results for the use of hybrid low-thrust propulsion. The results are created for a range of solar sail lightness numbers, ranging from $\beta_0 = 0.01$ to $\beta_0 = 0.1$ with a step size of 0.01. The results for $\beta_0 = 0.01$ are generated using the minimum propellant, pure SEP transfers of Figure 6 and Figure 7 as initial guess, while subsequent values for β_0 use the results for previous values of β_0 as initial guess.

The results for all test cases (i.e. constant and variable altitude pole-sitter orbits and short and long duration transfers) are shown in Figure 10 and Figure 11, where Figure 10 provides detailed results for the short duration transfer to the constant altitude pole-sitter and for $\beta_0 = 0.02$, while Figure 11 only provides the main outcomes for each of the test cases.

Inspecting the results for the short transfer between the constant altitude pole-sitter orbits in Figure 10 shows an interesting, but to be expected, change in the shape of the trajectory when adding a solar sail to the SEP thruster, see Figure 10a. The trajectory switches from a Sun-ward trajectory for the pure SEP case to an Earth-ward trajectory, clearly because in that way the required acceleration is more aligned with the Sun vector direction, the ideal for a solar sail. Furthermore, Figure 11e shows the improvements that hybrid low-thrust propulsion can establish over the pure SEP case for this particular case. It shows that, by increasing the sail lightness number, hybrid low-thrust propulsion allows for significant propellant mass savings, while also increasing the observation time per Pole. Moreover, if the lightness number is increased far enough, the required SEP propellant mass is zero and the transfer can be performed using only the solar sail. However, the corresponding sail lightness numbers are rather high for current technology. For instance, the Japanese solar sail demonstrator mission IKAROS[20] flew a sail with an area of 400 m^2 on a 307 kg spacecraft, leading to a sail lightness number of $\beta_0 = 0.000997$. Similarly, NASA's NanoSail-D[21] included a 10 m^2 sail for a 4 kg spacecraft, which corresponds to a sail lightness number of $\beta_0 = 0.003825$. Figure 11e therefore clearly shows the potential of hybrid low-thrust propulsion as transition phase between pure SEP and pure solar sail missions: it enables a reduction of the propellant mass with respect to the pure SEP case, while enabling a mission that would require far-future sail technology if the mission would be conducted using only a solar sail.

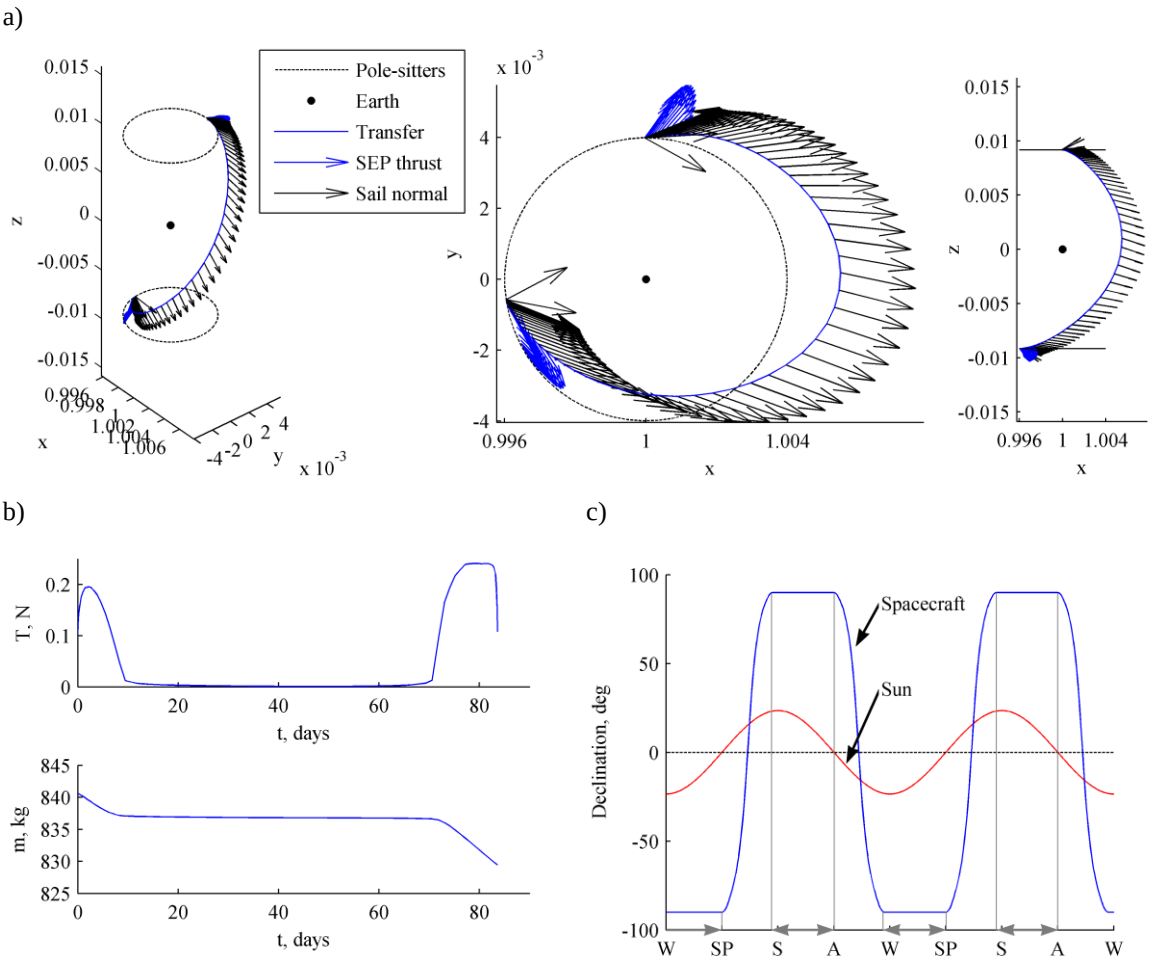

Figure 10 Hybrid propulsion, minimum propellant, short transfer between constant altitude pole-sitters for β_0 = 0.02. Transfer in CR3BP reference frame (a), thrust and mass profiles (b) and declination plot (c).

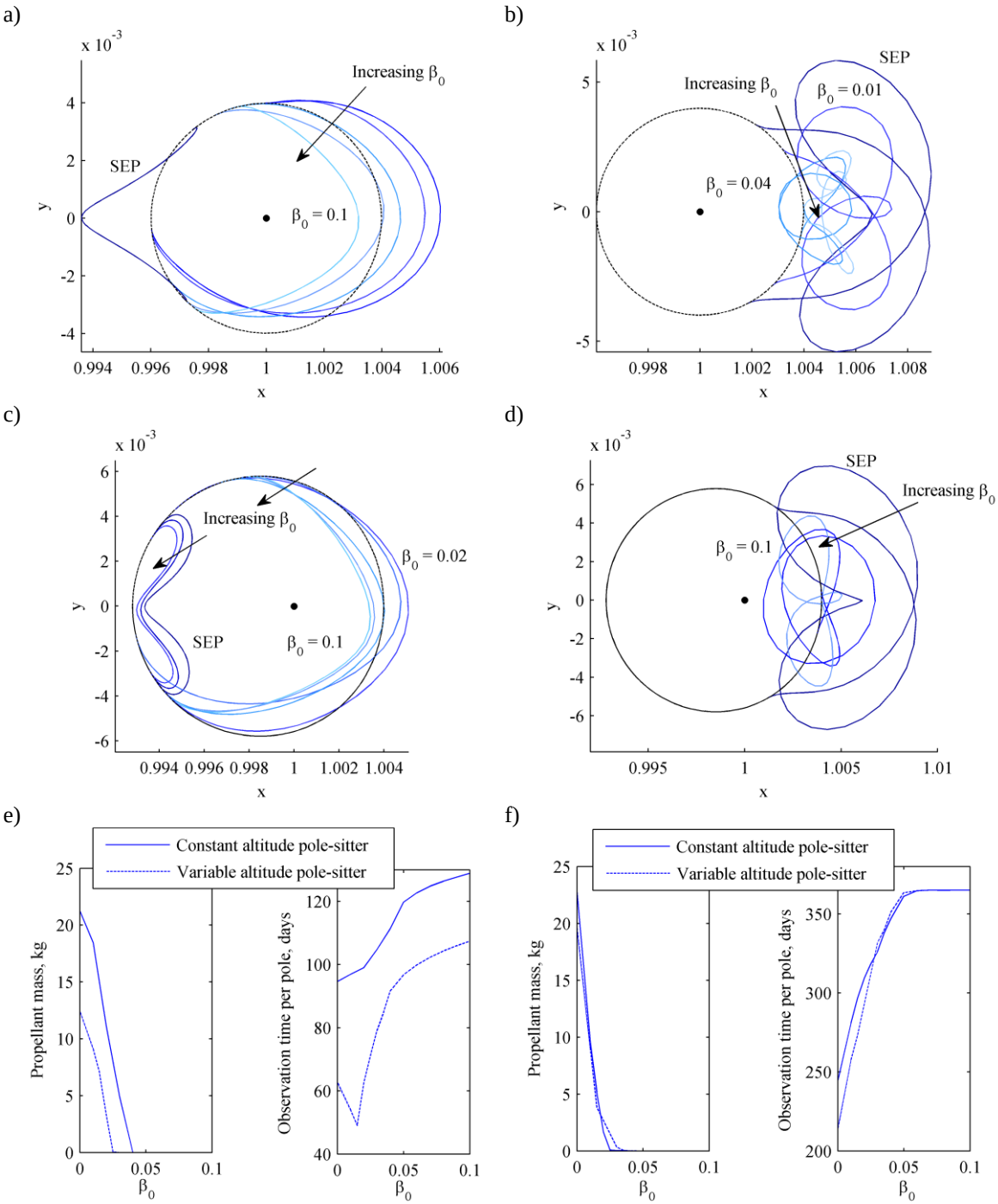

Figure 11 Hybrid propulsion, minimum SEP propellant transfers for different values of the sail lightness number β_0. Short (a, c and e) and long (b, d and f) transfer between constant and variable altitude pole-sitters.

Inspecting the results for the other test cases in Figure 11 shows a similar behavior. In general, increasing the sail lightness number results in a decrease in the propellant consumption and an increase in the observation time. The only exception to this is the short duration transfer between the variable altitude pole-sitter orbits for which Figure 11e shows that for small sail lightness numbers the decrease in propellant

consumption is accompanied by a decrease in the observation time. The explanation for this anomaly can be found in Figure 11c, which shows that the switch from a Sun-ward to an Earth-ward trajectory (that provided the longer observation times for the short duration transfer between constant altitude pole-sitters) occurs for $\beta_0 = 0.02$. Apparently, for smaller values of the sail lightness number, a continuation of the pure SEP transfer at the Sun-ward side of the pole-sitter orbit is more convenient from a propellant consumption point of view. This observation was confirmed by optimizations where the transfer was forced into an Earth-ward trajectory, which showed an increase in the propellant consumption.

Note that the optimizations considered in this section only minimize the SEP propellant consumption. Therefore, improvements in the observation time could possibly be established by considering the objective function in Eq. (18). Finally, also note that in all cases of Figure 11 the amount of propellant required to perform the transfer is smaller than the propellant required to remain in the pole-sitter orbit during the time it takes to perform the transfer.

NON-IDEAL SAIL THROUGH FEEDBACK CONTROL

The transfers presented in the previous sections are highly sensitive to perturbations and small changes in the initial conditions. Therefore, it is unrealistic to assume that the same control profile can be used in the real world, due to a number of contingencies and forces that are not completely modeled; for the hybrid transfers, one of the most important is the solar sail acceleration model. The solar sail modeled in Eq. (3) is ideal, in the sense that it assumes perfectly specular and complete reflection of the photons on the sail surface. As a result, the sail acceleration is aligned with the sail normal. In reality, however, a number of effects influence both the magnitude and the direction of the sail acceleration. First of all, the material is not perfectly reflective, but part of the photons are scattered, part are absorbed, and for thin membranes, part transmitted. Moreover, re-emission itself shall be considered. Finally, the surface of the sail may not be perfectly flat, due to imperfections in the fabrication and in the deployment, generating a number of wrinkles. Accurate modeling of all these effects was extensively studied in the literature;[22] nevertheless, they go beyond the scope of this section. For this paper, we will assume the following model,[23] known as optical sail, which takes into account specular reflection and absorption of the photons (scattered reflection and emission by re-radiation are neglected):

$$\mathbf{a}_s = \frac{1}{2}\beta_0 \frac{m_0}{m} \frac{\mu_S}{r_1^2} \left[g \cos\alpha \hat{\mathbf{n}} + h \sin\alpha \hat{\mathbf{t}} \right] \cos\alpha \tag{19}$$

This formula highlights that the absorption generates an acceleration component, $\hat{\mathbf{t}}$, that is tangential to the sail surface, in the plane of the Sun vector (see Figure 12). α is the so-called cone angle, i.e. the angle between the Sun vector $\hat{\mathbf{r}}_1$ and the sail normal $\hat{\mathbf{n}}$. The two coefficients *g* and *h* are functions of the optical properties of the sail surface. We will model the system assuming the following values for the coefficients: $g = 1.875$; $h = 0.125$, consistent to what is described in Reference 6, and the values are taking into account a sail of reflectivity coefficient 0.9 and the fact that 5% of the sail area is covered with thin film solar cells (reflectivity 0.4) for the generation of the power required by the SEP thruster.

The dynamics that will be used in this section to propagate the spacecraft states is the one in Eq. (3), but making use of the solar acceleration in Eq. (19). Because of this, it is obvious that the control profiles of the previous sections (named 'reference'), which were found considering an ideal sail, cannot control the spacecraft optimally under the new dynamics, and control is necessary. A feedback control loop is designed and implemented in the form of a linear quadratic regulator, which provides an additional control component that is added to the reference acceleration. Details of this implementation are subject of another paper.[24] We foresee that only the SEP thruster will be used for the feedback control in order to guarantee the controllability of the system and for a quick response to the required control.[24] Therefore, the control variables are the three Cartesian components of the SEP thrust vector. The sail attitude will follow the reference control throughout the transfer.

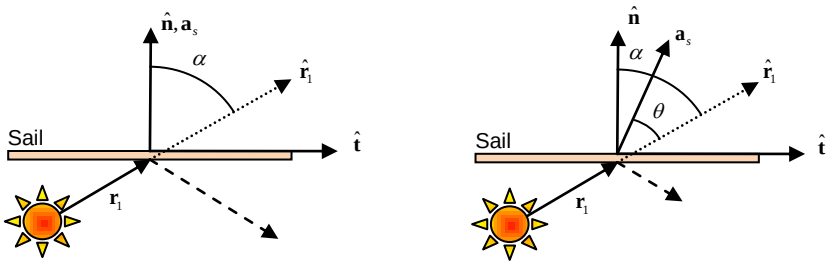

Figure 12 Schematics of an ideal sail model (a) and an optical sail model (b)

The feedback control is computed at each instant of time during the transfer, linearizing the system around the current state, assuming a control proportional to the state error, and solving the well-known Riccati equation. This type of control is effective under the assumptions that, at any instant of time, the real states are not too far from the reference ones (due the linear approximation), and that the reference signal does not vary quickly in time (as the linearized system is assumed time-invariant). The weight coefficients were determined by trial and error. Despite the fact that the dynamics of the system used for the propagation of the equations of motion will use the non-ideal sail model in Eq. (19), the linear quadratic regulator will assume an ideal sail (Eq. (3)). This is done to prove, in one specific case, that the control loop maintains the spacecraft close to the reference conditions, despite different and unknown dynamics acting on it.

The following figures, from Figure 13 to Figure 15, show the results of the feedback control, applied to two reference hybrid transfers between constant altitude pole-sitters: a short transfer with $\beta_0 = 0.02$ and a long transfer with $\beta_0 = 0.05$. These two cases are representative of the whole set of hybrid transfers that were found above.

Figure 13 and Figure 14 show the states and the thrust for each transfer case, respectively. For each figure, plots in (a) represent the state error, i.e. the difference between the real states and the reference states; plots in (b) are a comparison between the reference thrust magnitude and the total thrust magnitude when feedback is applied. For the short transfer with $\beta_0 = 0.02$, the position is confined within 2000 km and the velocity within 2 m/s from the reference. The additional fuel required for the feedback control is less than 2 kg, which still results in a better performance of the hybrid transfer over the pure SEP case, see Figure 11e. The two thrust arcs at the beginning and end of the transfer are maintained, while low-magnitude thrusting is added in the long coast arc in the middle. Worse, but still acceptable, performances are obtained for the case of the long transfer with $\beta_0 = 0.05$: here the position error is of order 10,000 km and the velocity of 15 m/s (however the arrival conditions are met more precisely). The additional mass required is approximately 7.4 kg. Again, even including this additional propellant mass, the hybrid transfer still outperforms the pure SEP case, see Figure 11f. In this transfer, even if the reference is completely ballistic, it requires a sensible additional thrust across the transfer. This is explained considering the fact that the sail, with a high lightness number, is providing all the necessary thrust, and therefore a change in its characteristics affects the transfer considerably. This also explains the higher fuel consumption that is needed by the feedback control. It is also important to underline that, of all the additional propellant that is required by the feedback control loop, only part of it is used to compensate the solar sail acceleration. Some propellant is used to counteract the instability of the transfer, instability that arises even without any perturbation, but just integrating the equations of motion.

Finally, Figure 15 shows the trajectories for the two cases. The reference trajectory (red line) is the one found by PSOPT considering an ideal sail. The red line is the trajectory found by propagating the initial conditions and the reference control considering a dynamics with an optical sail; no feedback control is used here, and it appears that in the short transfer (Figure 15a) the spacecraft terminates very far from the target pole-sitter orbit, while for the long transfer (Figure 15b) the trajectory diverges completely from the reference conditions. Instead, when the feedback control is used (green line), the trajectory closely follows the reference.

To conclude this section, note that a tighter control is also possible, at the cost of increased fuel consumption and increased oscillations in the feedback control signal (which can cause problems due to rapid thrust modulation and slew maneuvers required).

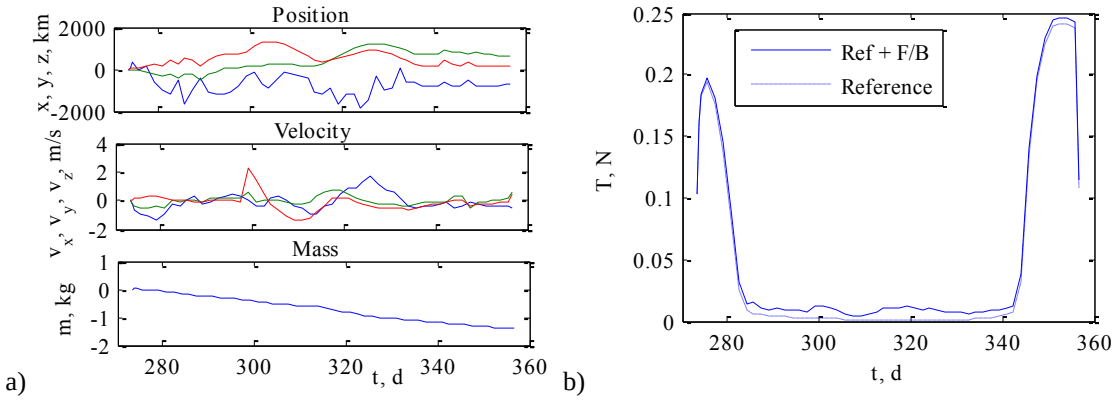

Figure 13 SEP feedback control on the hybrid short transfer, β_0 = 0.02. (a) Error between real states and reference states. (b) SEP thrust magnitude with and without feedback control.

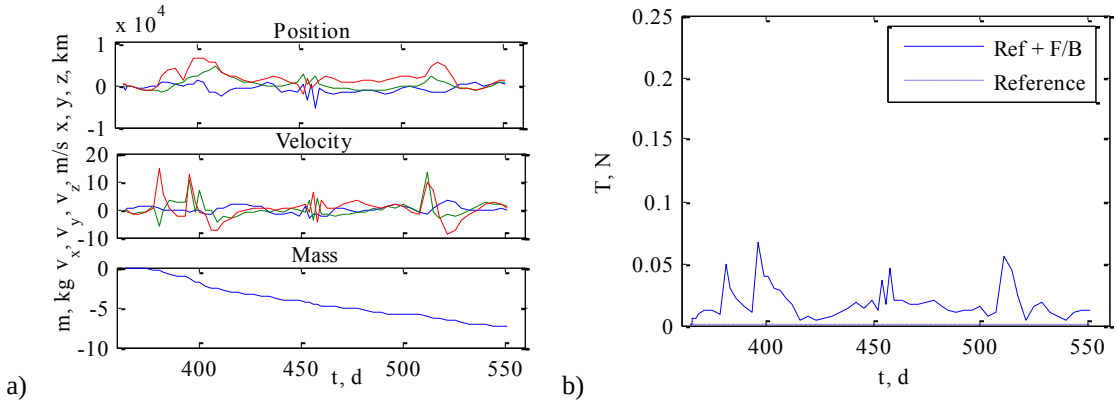

Figure 14 SEP feedback control on the hybrid long transfer, β_0 = 0.05. (a) Error between real states and reference states. (b) SEP thrust magnitude with and without feedback control.

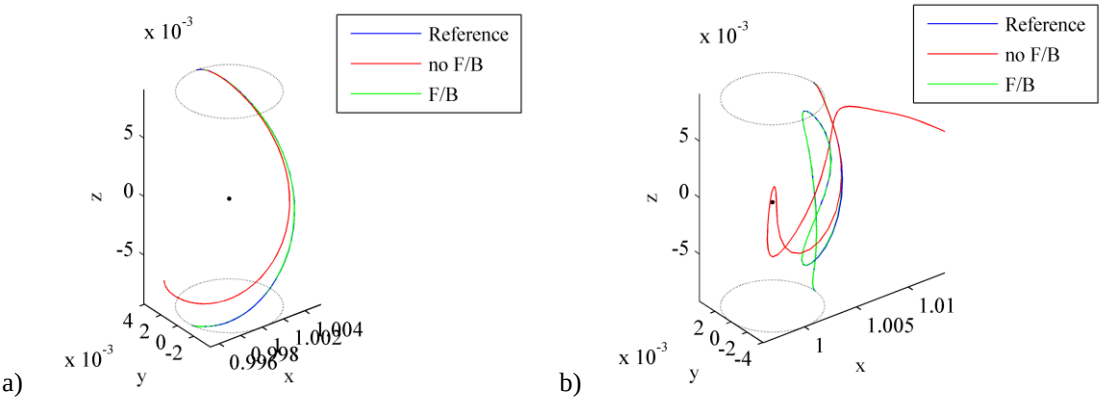

Figure 15 Comparison between reference trajectory, trajectory with optical sail without feedback control and with feedback control. (a) β_0 = 0.02, short transfer. (b) β_0 = 0.05, long transfer.

CONCLUSIONS

In this paper transfers between pole-sitter orbits above the North Pole and South Pole have been investigated, where a pole-sitter orbit follows the Earth's polar axis during the year. However, to limit the re-

quired thrust-induced acceleration to maintain the pole-sitter position, the Earth-spacecraft distance is quite significant and sufficient resolution of the observations can only be achieved in the visible part of the electromagnetic spectrum. However, due to the tilt of the polar axis, the polar regions are alternately situated in darkness which limits the scientific return. The transfers considered in this paper therefore allow for observations only in light conditions and can additionally allow for the observation of both the North and South Poles with one single spacecraft during one single mission. Two types of propulsion system have been investigated for performing the transfer, including pure solar electric propulsion (SEP) and a hybridization of SEP and solar sailing. For both propulsion strategies the optimal control problem has been defined and initial guesses have been produced through a shape based approach. Through the use of two different sets of time constraints, two different types of transfers could be defined: a short duration transfer where the spacecraft visits both the North and South Poles every year and during light conditions only and a long duration transfer where the spacecraft visits the North and South Poles every three years, resulting in much longer observations (though partially in dark conditions). Results have been produced using a direct optimization method based on pseudospectral transcription and two test cases have been considered: transfers between 0.01 AU constant altitude pole-sitter orbits and between 0.01 – 0.018 AU variable altitude pole-sitter orbits. For instance, the short duration transfer between constant altitude pole-sitter orbits requires a propellant mass of 21.26 kg and allows for 94.6 days of observation. This propellant consumption is less than the propellant consumed if the spacecraft would maintain its pole-sitter position. The transfer to the variable altitude pole-sitter orbits requires slightly less propellant but also the observation time decreases. Compared to the long duration transfer, the short transfer is more fuel optimal, but the long duration transfer allows for much longer observation times. For all test cases, the time spent above each of the Poles could be increased by adding this performance indicator to the objective function through a weighted sum approach. This led to an increase in the observation time of 32 to 151 days, depending on the test case considered, at the cost of an increase in the propellant mass of 16.9 to 49.4 kg. The results for the use of hybrid low-thrust propulsion showed that hybrid propulsion allows for significant propellant mass savings with respect to the pure SEP case, while increasing the observation time in almost all cases. These propellant mass savings increase for increasing values of the sail lightness number and for large enough lightness numbers, the transfer could even be performed using only the solar sail. However, for this, the lightness number would have to exceed current sail technology. As such, hybrid propulsion can be seen as a perfect tool for the transition between pure SEP and pure solar sail missions and to pull the technology development of sail technology. Finally, to take into account the non-ideal behavior of the solar sail, a feedback control loop was employed and demonstrated to be able to control the spacecraft, at the cost of additional propellant consumption, which varies from 2 to 8 kg, depending on the sail lightness number and the test case considered.

ACKNOWLEDGEMENTS

This work was funded by the European Research Council, as part of project 227571 VISIONSPACE, while attendance of the 22nd AAS/AIAA Space Flight Mechanics Meeting was funded through a Travel Grant of the Institution of Engineering and Technology (IET). Finally, the authors would like to thank Victor M. Becerra of the University of Reading for providing the software tool PSOPT freely and providing advice on its use.

REFERENCES

1. Schutz, B. E., Zwally, H. J., Shuman, C. A., Hancock, D., DiMarzio, J. P., "Overview of the ICESat Mission", *Geophysical Research Letters*, vol. 32, n. L21S01, 2005. doi: 10.1029/2005GL024009
2. Wingham, D. J., Francis, C. R., Baker, S., Bouzinac, C., Brockley, D., Cullen, R., de Chateau-Thierry, P., Laxon, S. W., Mallow, U., Macvrocordatos, C., Phalippou, L., Ratier, G., Rey, L., Rostan, F., Viau, P., Wallis, D. W., "CryoSat: A Mission to Determine the Fluctuations in Earth's Land and Marine Ice Fields", *Advances in Space Research*, vol. 37, p. 841-871, 2006.
3. Wertz, J. R., "*Mission Geometry; Orbit and Constellation Design and Management*", Space Technology Library, Microcosm Press/Kluwer Academic Publishers, El Segundo, USA/London, UK, 2001.
4. Anderson, P., Macdonald, M., "Extension of the Molniya Orbit Using Low-Thrust Propulsion", *21st AAS/AIAA Space Flight Mechanics Meeting, AAS 11-236*, New Orleans, USA, 2011.

5. Driver, J., "Analysis of an Arctic Polesitter", *Journal of Spacecraft and Rockets*, vol. 17, n. 3, p. 263-269, 1980. doi: 10.2514/3.57736
6. Ceriotti, M., McInnes, C. R., "Generation of Optimal Trajectories for Earth Hybrid Pole Sitters", *Journal of Guidance, Control, and Dynamics*, vol. 34, n. 3, p. 847-859, 2011. doi: 10.2514/1.50935
7. Ceriotti, M., McInnes, C. R., "Hybrid Solar Sail and Solar Electric Propulsion for Novel Earth Observation Missions", *Acta Astronautica*, vol. 69, n. 9-10, p. 809-821, 2011. doi: 10.1016/j.actaastro.2011.06.007
8. Lazzara, M. A., Coletti, A., Diedrich, B. L., "The Possibilities of Polar Meteorology, Environmental Remote Sensing, Communications and Space Weather Applications from Artificial Lagrange Orbit", *Advances in Space Research*, vol. 48, n. 11, p. 1880-1889, 2011. doi: 10.1016/j.asr.2011.04.026
9. Macdonald, M., McInnes, C. R., "Solar Sail Mission Applications and Future Advancement", *2nd International Symposium on Solar Sailing (ISSS 2010)*, New York, USA, 2010.
10. Mengali, G., Quarta, A. A., "Trajectory Design with Hybrid Low-Thrust Propulsion System", *Journal of Guidance, Control, and Dynamics*, vol. 30, n. 2, p. 419-426, 2007. doi: 10.2514/1.22433
11. Simo, J., McInnes, C. R., "Designing Displaced Lunar Orbits Using Low-Thrust Propulsion", *Journal of Guidance, Control, and Dynamics*, vol. 33, n. 1, p. 259-265, 2010. doi: 10.2514/1.45305
12. Heiligers, J., Ceriotti, M., McInnes, C. R., Biggs, J. D., "Displaced Geostationary Orbit Design Using Hybrid Sail Propulsion", *Journal of Guidance, Control, and Dynamics*, vol. 34, n. 6, p. 1852-1866, 2011. doi: 10.2514/1.53807
13. Baig, S., McInnes, C. R., "Artificial Three-Body Equilibria for Hybrid Low-Thrust Propulsion", *Journal of Guidance, Control, and Dynamics*, vol. 31, n. 6, p. 1644-1655, 2008. doi: 10.2514/1.36125
14. McKay, R. J., Macdonald, M., Vasile, M., Bosquillon de Frescheville, F., "A Novel Interplanetary Communications Relay", *AIAA/AAS Astrodynamics Specialist Conference*, AIAA-2010-7964, Toronto, Canada, 2-5 August, 2010.
15. Ceriotti, M., McInnes, C. R., Diedrich, B. L., "The Pole-Sitter Mission Concept: An Overview of Recent Developments and Possible Future Applications", *62nd International Astronautical Congress*, Cape Town, South Africa, 3-7 October, 2011.
16. McInnes, C. R., "Solar Sail Mission Applications for Non-Keplerian Orbits", *Acta Astronautica*, vol. 45, n. 4-9, p. 567-575, 1999.
17. Betts, J. T., "*Practical Methods for Optimal Control Using Nonlinear Programming*", Society for Industrial and Applied Mathematics (SIAM), Philadelphia, USA, 2001. p. 150.
18. Becerra, V. M., "Solving Complex Optimal Control Problems at No Cost with PSOPT", in *Proceedings of IEEE Multi-conference on Systems and Control*, Yokohama, Japan, 2010.
19. Wächter, A., Biegler, L. T., "On the Implementation of an Interior-Point Filter Line-Search Algorithm for Large-Scale Nonlinear Programming", *Mathematical Programming*, vol. 106, n. 1, p. 25-57, 2006. doi: 10.1007/s10107-004-0559-y
20. Tsuda, Y., Mori, O., Funase, R., Sawada, H., Yamamoto, T., Saiki, T., Endo, T., Kawaguch, J., "Flight Status of IKAROS Deep Space Solar Sail Demonstrator", *Acta Astronautica*, vol. 69, n. 9-10, p. 833-840, 2011.
21. Johnson, L., Whorton, M., Heaton, A., Pinson, R., Laue, G., Adams, C., "Nanosail-D: A Solar Sail Demonstration Mission", *Acta Astronautica*, vol. 68, p. 571-575, 2011.
22. Campbell, B. A., "An Analysis of Thrust of a Realistic Solar Sail with Focus on a Flight Validation Mission in a Geocentric Orbit", in *School of Engineering and Applied Science*. The George Washington University, Washington, DC, 2010.
23. McInnes, C. R., "*Solar Sailing: Technology, Dynamics and Mission Applications*", *Springer-Praxis Books in Astronautical Engineering*, ed. J. Mason, Springer-Verlag, Berlin, 1999.
24. Ceriotti, M., McInnes, C. R., "Hybrid Solar Sail and SEP Propulsion for Novel Earth Observation Missions", in *Proceedings of 61st International Astronautical Congress (IAC 2010)*, Prague, Czech Republic, 2010.